Behavior of Orthotropic Steel-UHPC Composite Bridge Deck under Cyclic Loading

Shi, Z.; Su, Qingtian; Veljkovic, Milan

Publication date
2022

Document Version
Final published version

Published in
IABSE Symposium Prague, 2022

IABSE Symposium Prague 2022
Challenges for Existing and Oncoming Structures
May 25-27 2022, Prague, Czech Republic

Behavior of Orthotropic Steel-UHPC Composite Bridge Deck under Cyclic Loading

Zhanchong Shi
Department of Bridge Engineering, Tongji University, Shanghai, China
Department of Engineering Structures, Delft University of Technology, Delft, The Netherlands
992364798@qq.ocm
Qingtian Su
Department of Bridge Engineering, Tongji University, Shanghai, China
sqt@tongji.edu.cn
Milan Veljkovic
Department of Engineering Structures, Delft University of Technology, Delft, The Netherlands
m.veljkovic@tudelft.nl

Contact: 992364798@qq.com

Abstract

In recent years, ultra-high performance concrete (UHPC) has been introduced in the design of orthotropic steel decks (OSD) to reduce the risk of fatigue cracking. To investigate the fatigue behaviour and fatigue damage process of the orthotropic steel-UHPC composite bridge deck, a full-scale specimen was designed and tested under cyclic loading. Test results show that the fatigue resistance of orthotropic steel-UHPC composite bridge deck satisfies the requirements of the designed vehicle load up to 2 million cycles with no cracks occurred in this phase. Rib-to-crossbeam weld and U-rib butt-welded connection are the two most vulnerable details to crack in OSD under cyclic loading. The fatigue resistance of U-rib bolted connection was investigated, and it is concluded that it performs better than that of U-rib butt-welded connection. The short-headed studs fractured under excessive cyclic loading and 5 types of the fatigue failure modes are identified. And the UHPC layer above the crossbeam exhibited limited number of cracks with the maximum crack width less than 0.05mm at the end of the cyclic, much beyond the requirements.

Keywords: composite deck; anchors; fatigue behaviour; short-headed studs; S-N curves.

1 Introduction

The conventional orthotropic steel bridge decks (OSD) are often used in large-span bridges, especially in cable-stay bridges and suspension bridges, for their higher strength, lighter self-weight, and more convenient installation. In operation practice, fatigue cracks of welded details in OSD have been observed worldwide, such as the Severn Bridge in the United Kingdom (Wolchuk 1990), the Throgs Neck Bridge in the United States

(Haight et al. 2005), Mafang Bridge (Cao et al. 2015) and Junshan Yangtze River Bridge (Wang et al. 2021) in China. Because the steel deck plate thickness is usually relatively thin, 12~16 mm, and is covered with a thin layer of 35~80mm of asphalt pavement, the local stiffness of OSD isn't large enough to satisfy fatigue requirements.

To solve or alleviate the severe fatigue cracking in OSD, one of the promising solutions is casting rebar reinforced high-performance concrete (Buitelaar et al. 2004) or ultra-high-performance concrete (Shao et al. 2013) to the top surface of OSD used to improve the local stiffness. The reinforced concrete layer is usually connected to the OSD by short-headed studs welded on the steel deck plate, and this kind of deck is usually named as the composite deck (Cao et al. 2017). The current investigations of orthotropic steel-UHPC composite deck usually focused on the verification test of the fatigue behaviour. The related fatigue failure test (Chen et al. 2019, Liu et al. 2019) and fatigue damage test are still limited. Additionally, the related assessment on the global fatigue performance of orthotropic steel-UHPC composite deck system is also still rare.

Faced at the current research status, a full-scale orthotropic steel-UHPC composite deck was designed and tested under cyclic loading. The fatigue damage process of the composite deck system was revealed. The fatigue performance of U-rib bolted connection and butt-welded connection were compared. Finally, the assessment of the global fatigue performance of the composite deck system was discussed.

2 Experimental program

2.1 Specimen design

A full-scale orthotropic steel-UHPC composite deck specimen was designed to investigate the fatigue behaviour of the deck system. The length, width and depth of the specimen were 8800mm, 1440mm and 392mm, respectively, as depicted in Figure 1. As shown, the steel deck plate with a thickness of 12mm was stiffened by two U-ribs and supported by three crossbeams. The top width，bottom width, depth and thickness of U-ribs were 360mm, 240mm, 300mm and 8mm, respectively. As the two U-ribs were connected by two types of connections, butt weld and high-strength bolts, at the location of 1000mm to the middle crossbeam in the longitudinal direction, so the two U-ribs were denoted as U_w and U_b (w means weld, b means bolt). The depth and thickness of cross-beam web were 450 mm and 12 mm, and the width and thickness of crossbeam flange were 200mm and 16mm. The UHPC layer had a thickness of 80mm and was reinforced by ϕ16 mm rebar mesh with spacing of 200 mm both in longitudinal and transverse directions. The stud connectors had diameter of 13 mm and height of 45 mm (after welding), so the studs were named as short-headed studs. Besides, the arrangement of short-headed studs was plotted in Figure 1 (b).

2.2 Material properties

The OSD was made of Chinese steel grade Q345. HRB400 was utilized for longitudinal and transversal rebar and ML15 was used for short-headed studs. The elastic modulus, yield strength and ultimate strength of steel grades are listed in Table 1. The UHPC used coarse aggregates with a maximum particle size of up to 8mm. The specific material compositions of UHPC is shown in Table 2. The 20 mm×0.25 mm (length*diameter) and 13 mm×0.2 mm (length*diameter) steel fibres were used to improve the tensile strength and toughness of UHPC. The mechanical properties of UHPC, including tensile strength according to Swiss recommendation (2016) and modulus of elasticity, cubic compress strength, first cracking strength under flexural tensile and flexural strength referring to Chinese Standard CECS13(2009), are summarized in Table 3. It should be noted that the material specimens were cured under natural curing condition for 28 days.

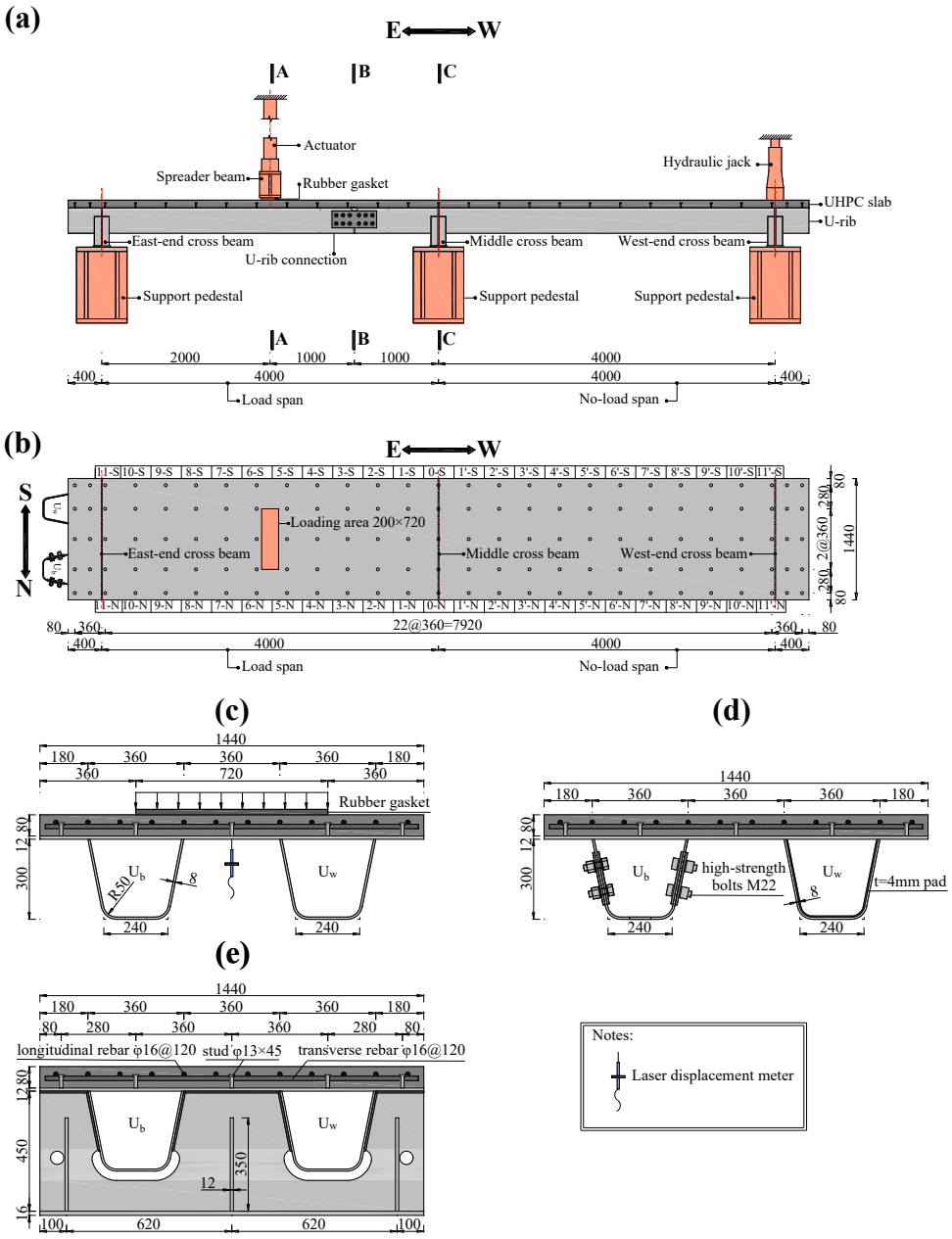

Figure 1. Details of full-scale specimen (unit: mm): (a) elevation view and setup; (b) arrangement of studs; (c) A-A cross section; (d) B-B cross section; (e) C-C cross section.

Table 1. Material compositions of 1 m^3 UHPC.

Item	Reactive powder	River sand	Basalt aggregate	Steel fibers	Superplasticizer	Water
Weight(kg)	1173	616	472	198	25.7	138
Size	micron	4-5mm	<8mm	hybrid	—	—

Table 2. Material properties of steel grades.

Material	*t* mm	*d* mm	E_s GPa	f_y MPa	f_u MPa
Q345	8	-	210	411	554
	12	-	210	370	511
HRB400	-	16	200	549	664
ML15	-	13	206	332	479

Note: E_s=modulus of elasticity; f_y=yield strength; f_u=ultimate strength.

Table 3. Material properties of UHPC

E_c GPa	f_{cu} MPa	f_{ct} MPa	$f_{cr,fl}$ MPa	$f_{ct,fl}$ MPa
48	108	7.45	11.53	22.38

Note: E_c, f_{cu}, f_{ct}, $f_{cr,fl}$, $f_{ct,fl}$ denote modulus of elasticity, cubic com-press strength, tensile strength, first cracking strength under flexural tensile and flexural strength, respectively.

2.3 Test setup and instrumentation

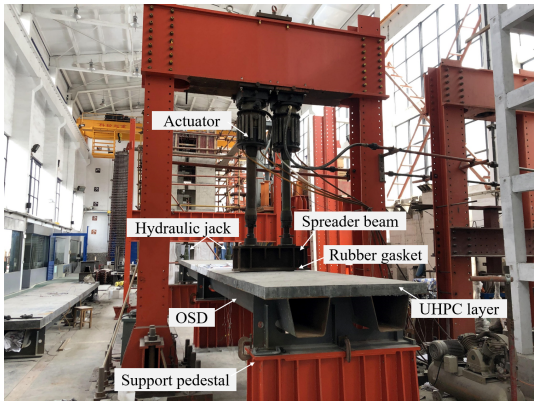

Figure 2. Test setup

Figure 1 (a) and Figure 2. illustrate the loading test setup. The specimen was placed and fixed on three steel support pedestals, and the support pedestals were attached to the ground via high-strength cement mortar. The actuator was placed at the mid-section in the span, and the cyclic load was applied from the actuator to the specimen through a spreader beam. To simulate the effect of vehicle wheel load, a 20 mm thick rubber with the size 200 mm by 720 mm was placed between the UHPC surface and spreader beam. To prevent vibration of the specimen under cyclic loading, two hydraulic jacks were applied to the top surface of the deck at the position of the west-end crossbeam.

The displacement of the loading point was measured by a laser displacement meter, as shown in Figure 3 (a). The measuring points of U-rib-to-deck-plate-to-middle-crossbeam welds were placed at an 8 mm distance from the weld root to capture the transversal strain, as shown in Figure 3 (b). The measuring points of the U-rib-to-crossbeam weld, as shown in Figure 3 (b) and Figure 3 (c), were placed at 8mm distance from the weld toe to capture the vertical strain. As shown in Figure 3 (b), the strain measuring points around middle-crossbeam cut-outs were used to capture the potential cracks around this area. Besides, the longitudinal strain of U-rib butt-welded connection and U-rib bolted connection was measured by strain gauges as shown in Figure 3 (d) and Figure 3 (e) respectively.

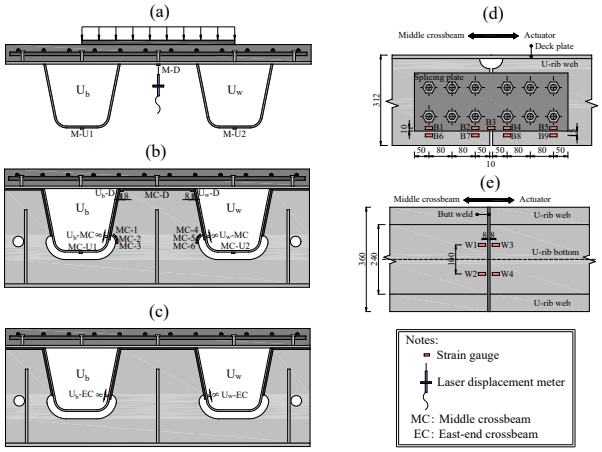

Figure 3. Instrumentation of specimen (unit: mm): (a) mid-span section of loading span; (b) section at middle crossbeam (MC); (c) section at east-end crossbeam (EC); (d) U-rib bolted connection; (e) U-rib butt-welded connection.

According to the design approach of the prototype bridge, the nominal tensile stress range of UHPC layer under vehicle wheel load was within 2.9 MPa. So, the designed loading protocol of the specimen was based on the tensile stress range of the top surface of UHPC layer above the middle crossbeam. The loading protocol is described in Table 4. As shown, the specimen was loaded at a constant load range (ΔP=P_{max}-P_{min}, P_{max} and P_{min} are the maximum and minimum load, respectively) in each phase. Phase I was designed to evaluate the fatigue behaviour of the composite deck in serviceability limit state, and the remaining phases were used to investigate the fatigue failure process of the specimen by increasing the load range. It should be noted that the east-end support pedestal was removed in phase VI, and the static load was applied at the same position to make the UHPC layer crack enough. Then in phase VII， the east-end crossbeam was removed back as phase I to phase V to investigate the fatigue cracking

behaviour of UHPC layer after pre-cracking statically loaded in phase VI. The loading frequency was kept at constant of 4 Hz during the whole cyclic loading phases. To investigate the stiffness degradation of the specimen, the static load was applied to the maximum load of the corresponding cyclic loading phases every 50000 cycles.

Table 4. Loading protocol

Phase	style	P_{min}~P_{max} (kN)	ΔP (kN)	N_i (×104)	f (Hz)
I	cyclic	271~405	134	200	4
II	cyclic	310~539	229	100	4
III	cyclic	560~807	247	160	4
IV	cyclic	798~1075	277	40	4
V	cyclic	421~730	309	50	4
VI	static	400	-	-	-
VII	cyclic	505~730	225	100	4

3 Experimental results and analysis

3.1 Fatigue cracks and stress range variation

In phase I, there was no obvious fatigue cracking occurred on the OSD, the UHPC layer and no interface debonding developed between the steel deck plate and the UHPC layer, indicating the composite deck system has sufficient fatigue resistance in the designed service life. As the load ranges and number of cycles increased, longitudinal cracks of U-rib initiating at U-rib-to-crossbeam welds and interface debonding between the steel deck plate and the UHPC layer developed. In general, there was no fatigue crack occurring at U-rib-to-deck-plate-to-crossbeam welds and at crossbeam cut-outs. Besides, the UHPC layer above the middle crossbeam sustained a slight fatigue crack with maximum crack width of less than 0.05mm during the whole cyclic loading phases.

3.1.1 Orthotropic steel deck

For fatigue-sensitive details in OSD, fatigue crack was firstly observed at lowest location of the U_w-rib-to-middle-crossbeam weld at 2.06 million cycles, see the stress range vs. number of cycles in Figure 5 . The crack initiated at the weld toe at the U_w-rib side and propagated upward along the weld toe until the vertical crack length up to 41mm at 3.65 million cycles. The vertical crack is shown in Figure 4 (a). Then the vertical crack stopped growing, and the crack started to propagated on the U_w-rib web in longitudinal direction. This longitudinal crack was named as Uw-MC-1# and is depicted in Figure 4 (b). The initiation and propagation of crack also could be captured by stress range evolution of the vertical strain gauge U_w-MC, and the curve of stress range to cyclic numbers is shown in Figure 5.

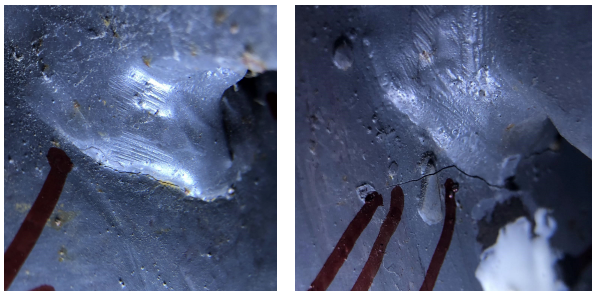

(a) (b)

Figure 4. Fatigue cracks of U_w-rib-to-middle-crossbeam weld: (a) vertical crack; (b)longitudinal crack.

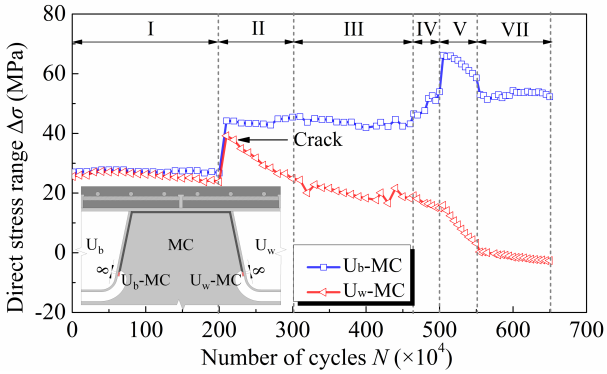

Figure 5. Stress range evolution of mearing points near U-rib-to middle-crossbeam welds.

As shown, the direct stress range of strain gauge U_w-MC started to decline at about 2.1 million cycles which was close to the time of visual observation of crack at 2.06 million cycles. The stress drop was the reason of stress relief caused by local cracking. It is clear that the stress ranges of measuring point U_b-MC were kept almost constant at each loading phase, indicating that there was no fatigue crack occurring near the weld. And this was validated by visual observation for no cracks were detected during the whole cyclic loading phases.

The evolution of crack length of Uw-MC-1# is shown in Figure 6. As shown, the growing rate of crack length from phase III to phase V was kept almost the same. The crack continued to develop until the crack reached a length of 33mm and was kept unchanged during the last cyclic loading phase.

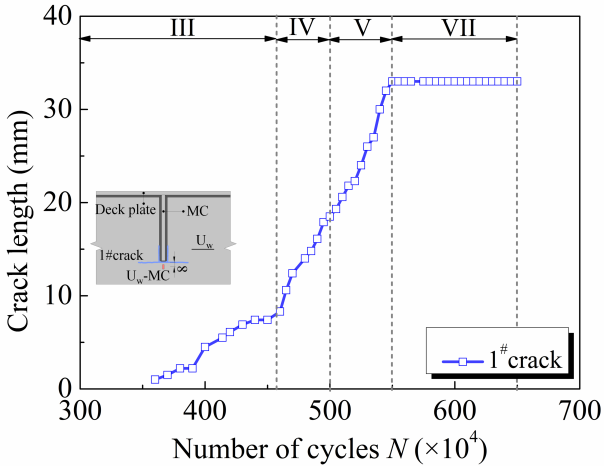

Figure 6. Evolution of crack length of U_w-MC-1#.

The fatigue crack with length of 29mm along the U-rib butt-welded connection at the bottom flange of U_w-rib was observed at 3.65 million cycles. The crack length developed quickly with the increasing of cyclic number at a constant load range in phase III, which could be seen from the evolution of crack length as depicted in Figure 7. To continue cyclic loading in the following phases, the cracked butt-weld was repaired by penetration welding and the related bottom flange of U_w-rib was stiffened by welding of two steel plates with a thickness of 16 mm over the weld at the end of phase III. The crack at butt welds and stiffening scheme are shown in Figure 8. The evolution of stress range of measuring points near the butt-welded connection is plotted in Figure 9. As plotted, the stress ranges of measuring points W2 and W4 dropped obviously at 3 million cycles, while that of measuring points W1 and W3 presented a slight climbing trend at the same time. And the crack was detected initiating from the area with welding initial defect (the weld presented crater compared with the adjacent full weld) near measuring points W2 and W4, and propagating to the direction of measuring points W1 and W3. After repaired and stiffened (from phase IV), the stress ranges of all measuring points stayed relatively constant until the end of the fatigue test, proving the effectiveness of the stiffening scheme.

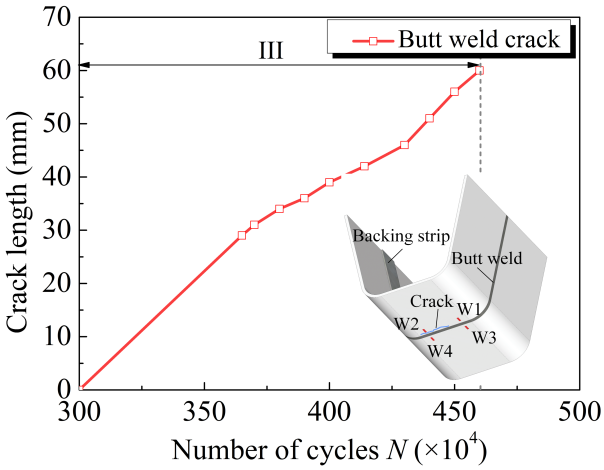

Figure 7. Evolution of crack length of butt-weld crack.

(a) (b)

Figure 8. U-rib butt-welded connection: (a) fatigue crack along the weld; (b) repairing and stiffening scheme.

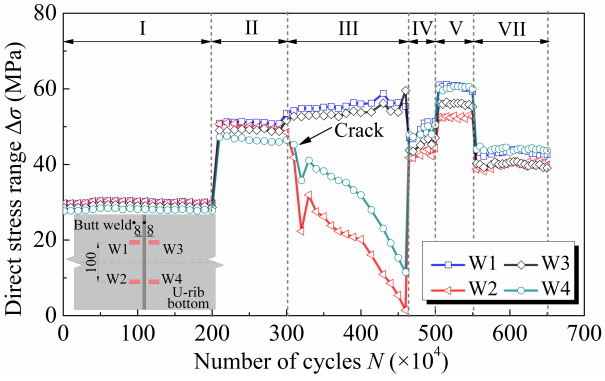

Figure 9. Evolution of stress range of measuring points of U-rib butt-welded connection.

No fatigue cracks were observed at the U-rib bolted connection. The evolution of stress ranges of measuring point at the bolted connection is plotted in Figure 10. As shown, the stress ranges of measuring points were kept almost equal at each cyclic loading phase. The U-rib bolted connection showed much better resistance to fatigue cracking than the U-rib butt-welded connection at the same

location and under identical loading conditions. There was no indication of fatigue damage at the bolted connection Therefore, the bolted connection is recommended for the connection of U-ribs on site considering the better fatigue resistance compared to the butt-welded connection.

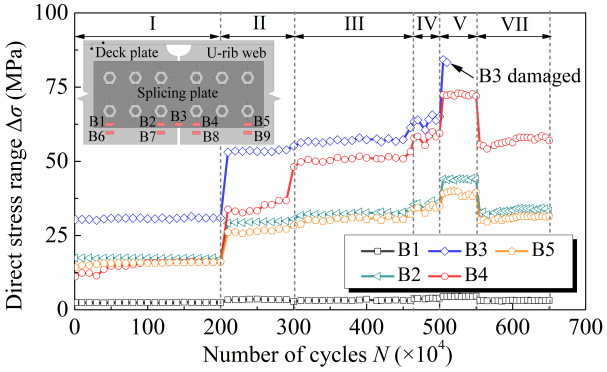

(a)

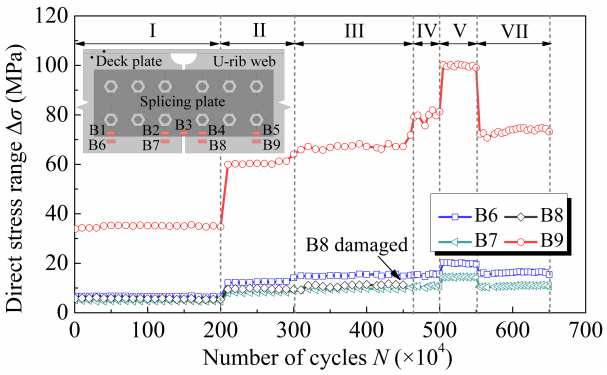

(b)

Figure 10. Evolution of stress range of measuring points of U-rib bolt-ed connection: (a) splicing plate; (b) U-rib.

3.1.2 Short-headed studs

It was difficult to detect the fatigue damage state of the short-headed studs embedded in the UHPC layer directly. Interface debonding between the steel deck plate and the UHPC layer was induced by fatigue damage of the short-headed studs. Therefore, interface debonding was chosen as failure criterion of studs. As shown in Figure 1 (b), take the mark "3-N" as an example, it denotes the inter-face located in the third stud column at the north side of the specimen. The first visible interface debonding occurred at the 3-N interface at 4.05 million cycles, as shown in Figure 11. Then more interfaces are separated with the increasing number of cycles. The marked interfaces occurring debonding and the corresponding fatigue life (number of cycles occurring debonding) are listed in Table 5.

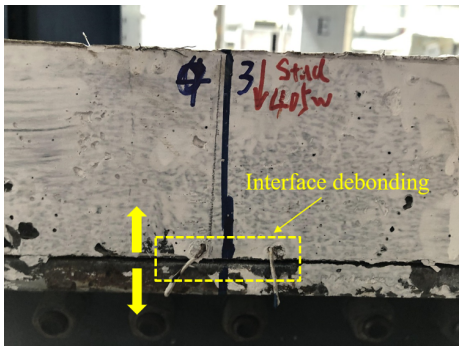

Figure 11. Interface debonding at 3-N.

Assuming the shear force at the interface was uniformly shared by all the short-headed studs at the same section of the span, the nominal shear stress range of the short-headed studs at each loading phase can be derived as:

$$\Delta\tau = \frac{\Delta V S_0 L(x)}{I_0 n_1 n_2 A_{sd}} \qquad (1)$$

where ΔV is shear force range of shear span; I_0 is the moment of inertia of the composite section; S_0 is the area moment of concrete section (converted into steel area) to the centre of gravity axis of composite section; $L(x)$ is the length of shear span; A_{sd} is the cross-section area of a single stud shank; n_1 is the number of stud rows (in trans-verse direction); n_2 is the number of stud columns (in longitudinal direction). For the shear span from east-end crossbeam to the actuator, ΔV, $L(x)$, n_1 and n_2 are (13 $\Delta P/32$), 2000 mm, 6 and 5, respectively; for the shear span from actuator to middle crossbeam, ΔV, $L(x)$, n_1 and n_2 are (19 $\Delta P/32$), 2000mm, 6 and 5, respectively; ΔP is load range summarized in Table 4.

$$\Delta\tau_e = \left[\frac{\sum N_i(\Delta\tau_i)^m}{N_f}\right]^{1/m} \qquad (2)$$

where $\Delta\tau_e$ is the equivalent constant amplitude nominal shear stress range; N_f is the fatigue life ; $\Delta\tau_i$ is shear stress range related to each loading phases; N_i is cyclic numbers related to shear stress range $\Delta\tau_i$; m is material constant (m=8 according to Eurocode 4). The calculated equivalent constant

amplitude shear stress range and the corresponding fatigue life of the short-headed stud connectors are listed in Table 5.

Table 5. Test results of short-headed studs.

Number	N_f (×10^4)	$\Delta\tau_e$ (MPa)	Number	N_f (×10^4)	$\Delta\tau_e$ (MPa)
3-N	405	187.9	4-S	498	198.9
2-S	414	188.7	5-N	539	211.4
2-N	420	189.2	10-S	525	142.2
1-N	429	189.9	8-N	539	144.7
1-S	429	189.9	8-S	539	144.7
3-S	429	189.9	9-N	539	144.7
0-N	481	196.1	9-S	539	144.7

Based on this beam test results listed in Table 5 and obtained from Chen's research (Chen er al. 2019), the shear fatigue S-N curves with 95% survival probability of short-headed studs used in the orthotropic steel-UHPC composite deck were established, as shown in Figure 12. Besides, Figure 12 also shows the comparison of S-N curves from the beam test and from the push-out test. It should be noted that the push-out test conducted by Cao (Cao et al. 2017) and Zhang (Zhang 2016) was also for short-headed studs embedded in a thin UHPC layer. As shown, the data points from the beam test lie above that from the push-out test, indicating that the short-headed studs have a larger shear fatigue strength in the beam test. This phenomenon was also validated in Roberts's fatigue test (Roberts et al. 1998) for normal size studs embedded in normal concrete slab. This result may be explained by the more pronounced shear stress distribution in the beam test than in the push-out test.

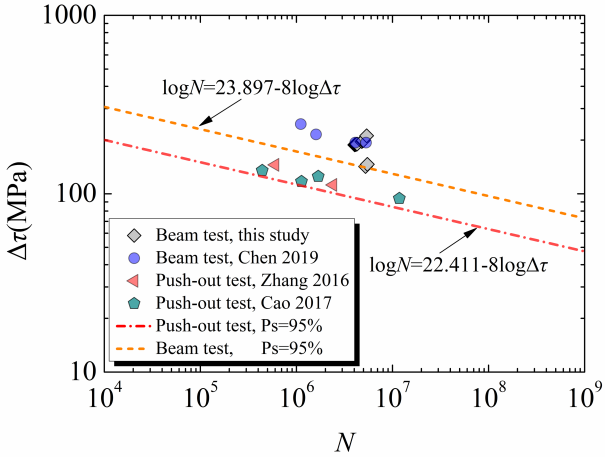

Figure 12. Comparison of shear fatigue S-N curves between the beam test and the push-out test.

The UHPC layer was removed by high-pressure water jet after the fatigue test to reveal the fatigue failure modes of the short-headed studs. The failures modes could be classified into 5 types, mode (a) to (d) and combined mode (da), (db) and (dc), as shown in Figure 13. Modes (a) to (c) are fatigue fracture occurring at the stud shank, mode d is the fatigue tearing off of the steel deck plate. The combined mode (da), (db) and (dc) are fatigue damage occurring both at stud shank and the steel deck plate. The fractured area of stud shank and steel deck plate could be divided into the smooth region caused by fatigue crack expansion and the rough area induced by static failure.

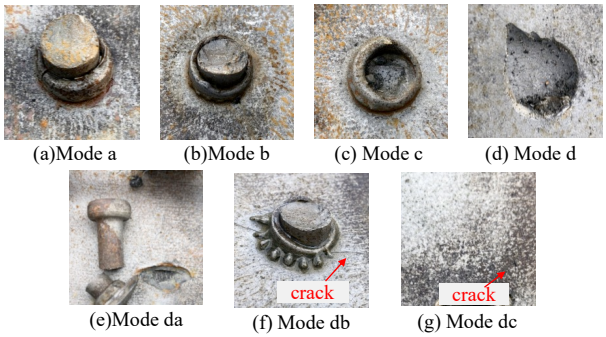

Figure 13. Fatigue failure modes of the short-headed studs.

3.1.3 UHPC layer

The UHPC layer above the middle crossbeam didn't exhibit severe crack as for the crack numbers and maximum crack width during the whole loading phases. Figure 14 depicts the crack distribution of UHPC layer above the middle crossbeam at the end of the final loading phases under the maximum load. As plotted, only several short and thin cracks emerged from phase I to phase V, with maximum crack width less than 0.04 mm. The main objective of static loading under simply supported cantilever condition in phase VI was to make the UHPC layer sustain severe crack and to investigate the fatigue behaviour of composite deck system when UHPC was damaged enough. The maximum crack width of 0.15 mm for UHPC layer above the middle crossbeam was obtained in phase VI, and more densely distributed cracks were developed. When the structural system was transformed from simply

supported cantilever system in phase VI to two-span continuous system in phase VII， most new cracks emerged in phase VI were missing. Besides, the maximum crack of UHPC layer was still 0.04mm in phase VII. In a word, the UHPC layer at the negative moment zone didn't suffer from severe fatigue damage during the whole cyclic loading phases. And the UHPC layer provided a sufficient stiffness for the composite deck consistently even under 2.3 times the designed live load range in phase V.

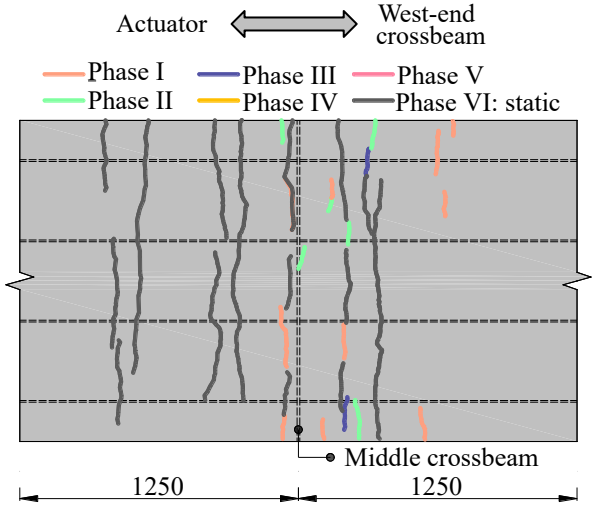

Figure 14. Crack distribution of UHPC layer in final phases.

3.2 Global stiffness response

The global mechanical properties of the specimen after cyclic loading could be showed by load-midspan deflection response under static loading. The static loading-midspan displacement relationships after a different set of the cyclic loading are plotted in Figure 15.

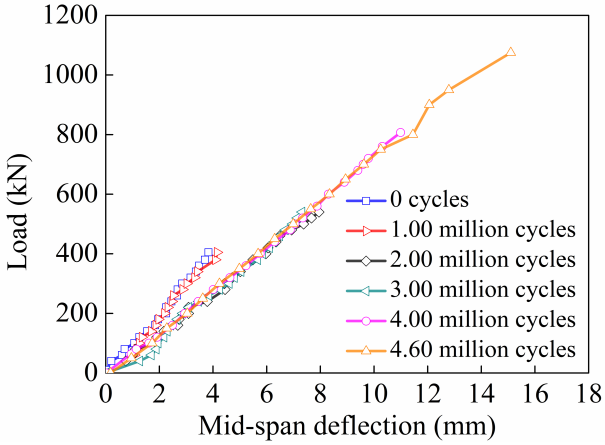

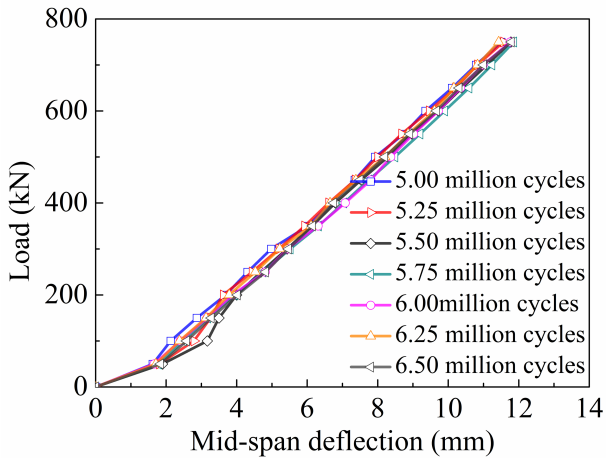

Figure 15. Load-midspan deflection response.

The analysis of the evolution of load-midspan deflection response should be linked to the fatigue damage of the orthotropic-UHPC composite deck. The crack on U_w-rib at U_w-rib-to-middle crossbeam welds firstly occurred at 2.06 million cycles, and the crack propagated to the length of 33mm to the end of the test. The crack on U-rib butt-welded connection was captured at 3.65 million cycles, and the crack propagation was pre-vented by repairing and stiffening scheme at 4.6 million cycles. During the propagation of fatigue cracks on OSD, shear interface debonding induced by fatigue fracture of short-headed studs emerged at 4.05 million cycles, and the interface debonding was expanding both in vertical and longitudinal directions until the end of the test. From Figure 15, the load-midspan deflection curves corresponding to different cyclic numbers were almost identical, indicating the fatigue damage of different components didn't affect the global stiffness.

4 Conclusions

(1) The full-scale orthotropic steel-UHPC composite deck satisfies the expected fatigue lifetime of the serviceability design live load.

(2) Under enlarged cyclic loading, the crack on U-rib initiated from the weld toe at the bottom of the U-rib-to-crossbeam weld firstly occurred. Then the crack on U-rib butt-welded connection initiated and propagated along the weld length, followed by shear interface debonding between steel deck plate and UHPC layer.

(3) The U-rib bolted connection showed much better fatigue resistance than the U-rib butt-welded connection under identical loading conditions and is recommended as the in-situ connection.

(4) The UHPC layer at the negative moment zone exhibits excellent fatigue cracking resistance in the composite deck system.

5 References

[1] Wolchuk R. Lessons from weld cracks in orthotropic decks on three European bridges. *Journal of Structural Engineering*. 1990; 116(1), 75-84.

[2] Haight R., Chang S., & Kushmock R. Orthotropic deck rehabilitation at the Throgs Neck Bridge. In Structures Congress 2005: Metropolis and Beyond (pp. 1-10)

[3] Cao J., Shao X., Zhang Z,, et al. Retrofit of an orthotropic steel deck with compact reinforced reactive powder concrete. *Structure and Infrastructure Engineering*. 2016; 12:3, 411-429.

[4] Wang Y., Shao X., Chen J., Cao J., & Deng, S. UHPC-based strengthening technique for orthotropic steel decks with significant fatigue cracking issues. *Journal of Constructional Steel Research*. 2021; 176, 106393.

[5] Buitelaar P., Braam R., & Kaptijn N. Reinforced high performance concrete overlay system for rehabilitation and strengthening of orthotropic steel bridge decks. *In Orthotropic Bridge Conference, Sacramento*, USA; 2004.(pp. 384-401).

[6] Shao X., Yi D., Huang Z., Zhao H., Chen B., & Liu M. Basic performance of the composite deck system composed of orthotropic steel deck and ultrathin RPC layer. *Journal of Bridge Engineering*. 2013; 18(5), 417-428.

[7] Cao J., Shao X., Deng L., & Gan Y. Static and fatigue behavior of short-headed studs embedded in a thin ultrahigh-performance concrete layer. *Journal of Bridge Engineering*. 2017; 22(5), 04017005.

[8] Chen S., Huang Y., Gu P., & Wang J. Y. Experimental study on fatigue performance of UHPC-orthotropic steel composite deck. *Thin-Walled Structures*. 2019; 142, 1-18.

[9] Liu Y., Zhang Q., Meng W., Bao Y., & Bu Y. Transverse fatigue behavior of steel-UHPC composite deck with large-size U-ribs. *Engineering Structures.* 2019*;* 180, 388-399.

[10] MCS-EPFL. Ultra-High Performance Fibre Reinforced Cement-based composites (UHPFRC) Construction material, dimensioning und application. Lausanne, Switzerland. 2016.

[11] China Association for Engineering Construction Standardization. Standard test methods for fiber reinforced concrete. China Plan Press, Beijing, China. 2009.

[12] Miner, M. A.. Cumulative damage in fatigue. *J. Appl. Mech*. 1945; 12(3): A159-A164.

[13] European Committee for Standardization. EN1994 Eurocode 4: Design of composite steel and concrete structures-Part 2: Composite bridges. Brussels, Belgium. 2005.

[14] Zhang S. Basic performance of a lightweight composite bridge deck with open ribs. Master's Thesis, Hunan University, Changsha, China. 2016.

[15] Roberts T. M., & Dogan O. Fatigue of welded stud shear connectors in steel–concrete–steel sandwich beams. *Journal of Constructional Steel Research*. 1998; 45(3), 301-320.